# Effects of Charging Rates on LiNi<sub>0.6</sub>Mn<sub>0.2</sub>Co<sub>0.2</sub>O<sub>2</sub> (NMC622)/Graphite Li-ion Cells

Xianyang Wu<sup>a,b</sup>, Yaocai Bai<sup>a</sup>, Zhenglong Li<sup>a</sup>, Jue Liu<sup>c</sup>, Kejie Zhao<sup>b</sup>, Zhijia Du<sup>a,z</sup>,

a Energy and Transportation Science Division, Oak Ridge National Laboratory, Oak Ridge, TN 37830, USA

b School of Mechanical Engineering, Purdue University, West Lafayette, IN 47907, USA
c Neutron Scattering Division, Oak Ridge National Laboratory, Oak Ridge, TN 37830, USA
-corresponding to Zhijia Du (duz1@ornl.gov, +1-(865)574-7519)

#### **Abstract**

Enabling fast charging capability of lithium-ion battery is of great importance to widespread adoption of electric vehicles. Increasing the charging rates from state-of-the-art 2C (30 minutes) to 6C (10 minutes) requires deep understanding on the cell aging mechanism. In this study, 400 mAh pouch cells are cycled at 1C, 4C and 6C charging rates with 1C discharging rate. Capacity fading, cathode structural changes, Li inventory loss, electrolyte composition changes and Li plating on graphite electrodes are thoroughly studied by various characterization techniques. The rapid capacity fading in cells at 6C charging rate is mainly due to Li inventory loss from cathode structure and metallic Li plating on graphite electrode at higher charging rate. Post-mortem analysis also revealed changes in electrolyte such as increased salt molarity and transesterification during fast charging.

# Notes

This manuscript has been authored by UT-Battelle, LLC under Contract No. DE-AC05-00OR22725 with the U.S. Department of Energy. The United States Government retains and the publisher, by accepting the article for publication, acknowledges that the United States Government retains a non-exclusive, paid-up, irrevocable, world-wide license to publish or reproduce the published form of this manuscript, or allow others to do so, for United States Government purposes. The Department of Energy will provide public access to these results of federally sponsored research in accordance with the DOE Public Access Plan (http://energy.gov/downloads/doe-public-access-plan).

#### 1. Introduction

The development of Li-ion cells with fast-charging capability is critical to further progress the widespread of electric vehicles [1]. The charging of an electric vehicle should ideally cost a similar amount of time compared to refueling a gasoline engine vehicle, which is 15 minutes or less. High-power Li-ion cells with thin electrodes are capable of recharging in short time (10 $\sim$ 15 minutes). However, these cells have lower energy density and would lead to higher cell cost compared to state-of-the-art high energy density cells. A calculation by Ahmed et al. found a 10 minutes fast charging cell design with 19  $\mu$ m thick anode increase the cell cost sharply to \$ 196/kWh, compared to \$107/kWh with 87  $\mu$ m thick anode capable of 47 minute charging [2]. In the high energy density Li-ion cells, fast charging can adversely lead to degradation in battery safety, energy density and cycle life.

Li plating has been identified as one of the most critical issues affecting battery performance [2–7]. It occurs on the surface of the graphite electrode when large overpotentials in a cell decrease the local potential to below 0 V (vs. Li<sup>+</sup>/Li)[8–10]. Gallagher et al. have systematically studied the effect of electrode loading (thickness) and charging rate on Li plating [11]. It was found a relatively moderate charging rate of 1.5 C (40 minutes charging) can have significant impact on Li-ion cells with 3.3 mAh/cm<sup>2</sup> loading, leading to capacity decrease and metallic Li deposition. Li plating can result in irreversible capacity loss due to the removal of active Li inventory in the cell [12]. Fully discharging of the cells with Li plating even at a low rate did not strip the deposited Li back to the positive electrode [11]. Another issue with Li plating is its high tendency to form dendrites with high surface area, which increase the parasitic reactions with electrolyte, forming isolated (dead) lithium, and thus reducing the Coulombic efficiency [13–15]. Li dendrite would also short the cell, cause catastrophic failure of the battery, and even inducing fatal safety hazards [16–19].

Fast charging can also lead to rapid temperature rise from the high heat generation rate due to the large current applied to the cell. With embedded thermal couple in a 2-Ah pouch cell, Huang et al. observed the temperature of the cell rose from room temperature (23 °C) to 38 °C under 5C charging rate and 45 °C under 7C within 5 minutes [20]. This increased temperature can result in a decrease of the cell resistance to improve kinetics. Yang et al. have shown the cell performance during fast charging can be improved by intentionally heat the cell by internal heaters [21]. However, performance degradation can be aggravated by exposing the cell to elevated operation temperature. This is because parasitic reactions, like SEI growth, are intensified with increased temperatures [22]. Increase in the temperature can also worsen other unwanted reactions such as transition metal dissolution and binder decomposition [23,24].

In the present study, we study the effects of fast charging (+1C, +4C and +6C) on the capacity fading, electrode microstructural changes and electrolyte changes in LiNi<sub>0.6</sub>Mn<sub>0.2</sub>Co<sub>0.2</sub>O<sub>2</sub> (NMC622) /graphite pouch cells. A detailed post-mortem analysis is performed to study the aging under different fast charging rates via electrochemical testing, neutron powder diffraction, inductively coupled plasma atomic emission spectroscopy (ICP-OES), gas chromatography–mass spectrometry (GC-MS), etc.

#### 2. Experiments

Electrodes and pouch cells with capacity of 400 mAh were prepared in a dry room (dew point < -50 °C) at the DOE Battery Manufacturing R&D Facility (BMF) at Oak Ridge National Laboratory (ORNL). The cathode was NMC622 (Targray) electrodes with 2.3 mAh/cm<sup>2</sup> areal capacity loading and calendered to 30% porosity. The anode was graphite (Superior Graphite 1520T) electrodes with 2.6 mAh/cm<sup>2</sup> areal loading and calendered to 30% porosity. The electrolyte filled into the

pouch cell was 1.2 M LiPF<sub>6</sub> in ethylene carbonate (EC): ethyl methyl carbonate (EMC) 3:7 by weight (*soul*brain MI).

The cell cycling was carried out on a battery cycler, Maccor Series 4000, in an environmental chamber at 30 °C. The cells were cycled between 2.8 and 4.2 V with a constant voltage holding at 4.2 V (trickle charging). A total time limit was imposed to guarantee that the duration of the charging step did not exceed the intended time for each C rate (10 minutes for 6C charging, 15 minutes for 4C, and 1 hour for 1C charging). Half coin cells were built to test the Li inventory loss in cathodes. Both NMC622 cathode and graphite anode electrodes were punched from aged NMC622 pouch cells after disassembling in the Ar-filled glove box. The electrodes were then assembled into Li coin cells with Li metal as the counter electrodes. The electrolyte was fresh electrolyte, and the half coin cells were charged and discharged at a constant rate of C/10 between 2.5 V and 4.2 V.

NMC and graphite powder samples were collected from the electrodes after discharging the cell

to 2.0 V and disassembled in Ar-filled glove box. Room temperature neutron total scattering data were collected at the NOMAD beamline at the Spallation Neutron Source (SNS) at ORNL[25]. About 3.0 g powder sample was loaded into a 3 mm quartz capillary. The detectors were calibrated using scattering from a diamond powder standard prior to the measurements. The average structure refinements using neutron diffraction data were carried out in TOPAS Academic, version 6 [26]. The gas generation during fast charging cycles was studied by using Archimedes principle, similar to previous report [27]. The cells were hung below an analytical balance and suspended in silicone mechanical pump oil at room temperature. The test was carried out after 50 cycles and 200 cycles. The electrolyte after long-term cycling was analyzed by ICP-OES following a similar procedure reported by Thompson et al. [28]. The pouch cells after cycling were cut open in the dry room and

sealed in centrifuge tube, then they were centrifuged under 2000 rpm for 20 minutes to extract cycled electrolyte. The extracted liquid electrolyte ( $\sim 0.10~g$ ) was first diluted with  $\sim 20~g$  rams of 2 wt% HNO<sub>3</sub> with  $\sim 0.2~g$  CH<sub>2</sub>Cl<sub>2</sub> added for organic separation. The 1<sup>st</sup> diluted solution was then centrifuged under 2000 rpm for 30 minutes for fully extraction of Li<sup>+</sup> into the aqueous HNO<sub>3</sub> and phase separation. Then  $\sim 1~g$  of 1<sup>st</sup> diluted solution from the top layer was added into  $\sim 10~g$  2% HNO<sub>3</sub> and shaken for 15 minutes. The 2<sup>nd</sup> diluted solution was then analyzed using Agilent Technologies 5110 ICP-OES to obtain the different elemental concentrations.

GC-MS was used to analyze the composition changes in the electrolyte solvents after long term fast charging cycles. One drop of the recovered electrolyte from cycled pouch cell was diluted in polytetrafluoroethylene vials with ~15 mL of CH<sub>2</sub>Cl<sub>2</sub> and ~0.1 mL deionized water for the complete extraction of Li salts [28,29]. The vial was machine-shaken for 30 minutes in two directions and centrifuged for 30 minutes under 2000 rpm for complete separation. The organic layer (electrolyte solvents in CH<sub>2</sub>Cl<sub>2</sub>) was removed by diluting into CH<sub>2</sub>Cl<sub>2</sub> again, followed by another machine-shaken of 15 minutes. The organic layer was then analyzed by an Agilent 6850 GC-MS system. The GC inlet temperature is 250 °C with a split ratio of 1:10. Carrier gas was helium at a linear velocity of 1.5 mL/min. The column temperature started at 40 °C and ramped up to 250 °C at a heating rate of 8 °C/minute. The interface and ion source temperature for MS were 250 and 200 °C, respectively.

The morphology of the electrode was characterized by a scanning electron microscope (SEM, Carl Zeiss Merlin)

#### 3. Results and Discussion

**Figure 1**a shows the cycling performance of the NMC622/graphite pouch cell under different charging rates of 1C, 4C and 6C. The capacity shown on the Y-axis is based on the mass of the

cathode materials NMC622. The capacity retentions after 200 cycles (compared the 1<sup>st</sup> cycle) are 94.0%, 89.4% and 73.8% under 1C, 4C and 6C charging rate, respectively. **Figure 1**b shows the voltage curves of cells at the 1<sup>st</sup>, 50<sup>th</sup> and 200<sup>th</sup> cycles under different charging rates. During the 1<sup>st</sup> cycle, the capacities of the cell (corresponding to the mass of NMC622) are 164, 152 and 143 mAh/g under 1C, 4C and 6C charging rates, respectively. Huge polarization is observed with increasing the charge current from 1C to 6C. The capacity decreases under increasing charging current are due to the mass transport limitation in electrolyte and/or sluggish diffusion kinetics in graphite [11,30,31].

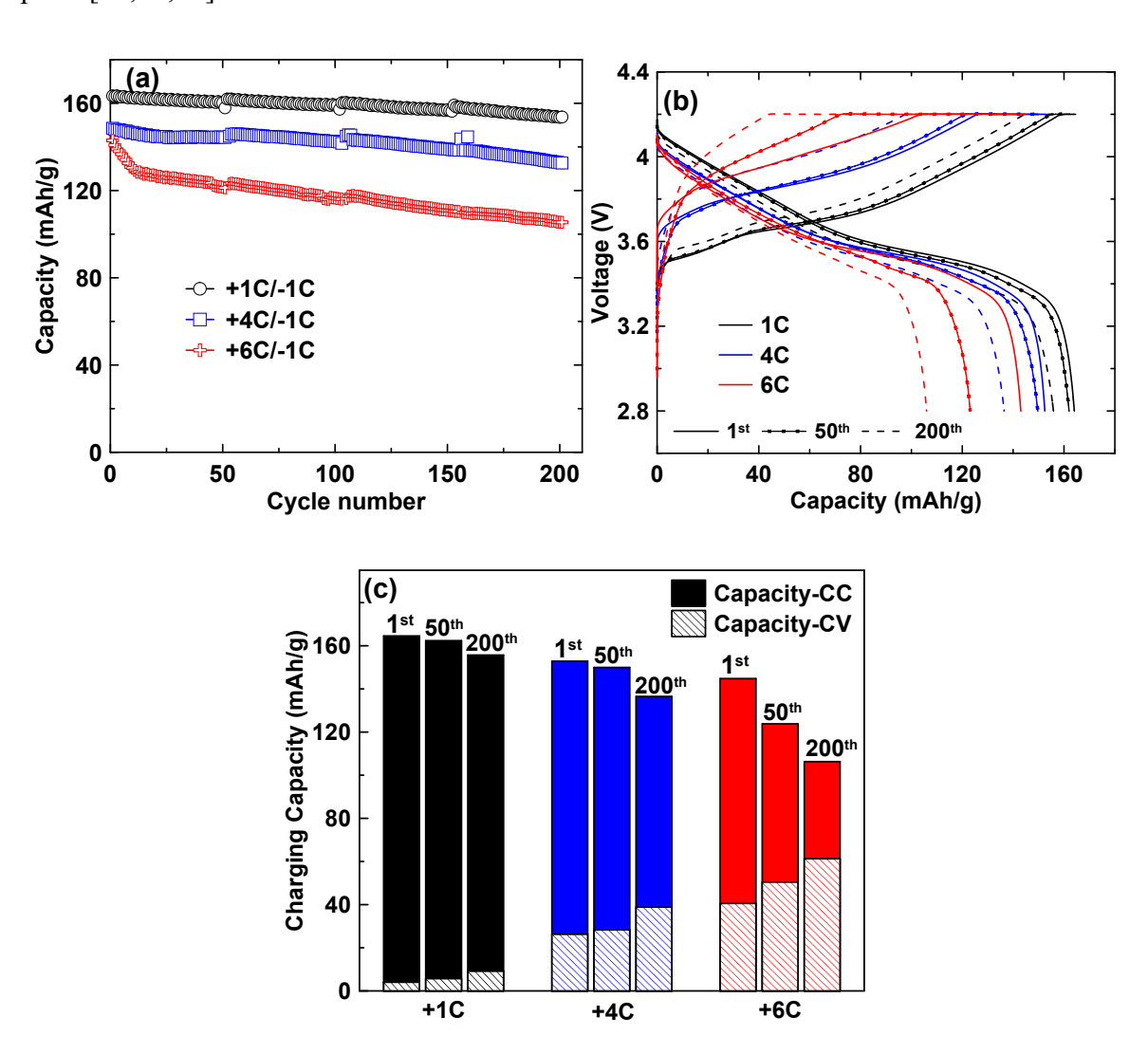
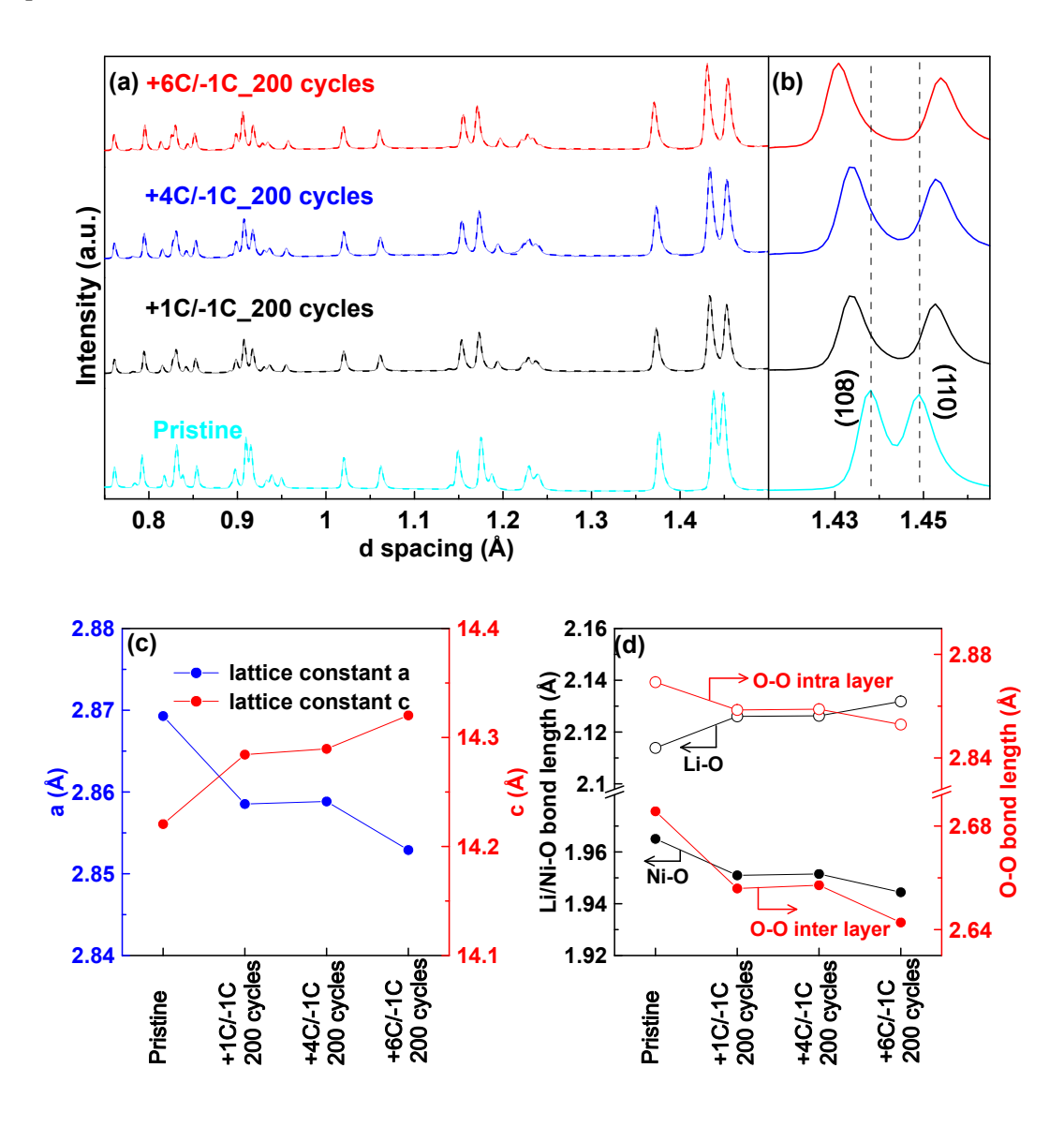


**Figure 1**. electrochemical performance of NMC622/graphite pouch cell under different charging rates. (a) cycling performance; (b) voltage curves at 1<sup>st</sup>, 50<sup>th</sup> and 200<sup>th</sup> cycle; (c) capacity from constant current charging and capacity from constant voltage charging at 1<sup>st</sup>, 50<sup>th</sup> and 200<sup>th</sup> cycle.

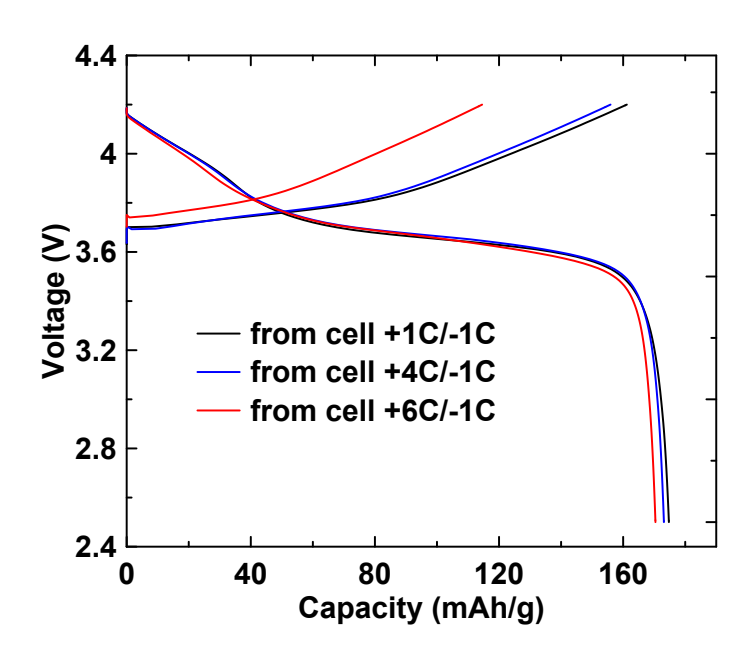
**Figure 1**c shows the capacities of the cells obtained within the specified time (60 minutes for 1C, 15 minutes for 4C and 10 minutes for 6C) from the 1<sup>st</sup>, 50<sup>th</sup> and 200<sup>th</sup> cycles. The capacities consist of capacity from the constant current (capacity-CC) charging and that from the constant voltage (capacity-CV) charging. The portion of capacity-CV in total capacity increases significantly with the increase of charging current. It also increases with the cycling number, indicating continuous aging and increasing polarization in the cell. Under 6C charging after 200 cycles, more than 50% of the total capacity is from capacity-CV. This high voltage operation has been reported to cause more degradation in Li-ion cells [32,33].

Figure 2a shows the bank 4 neutron diffraction patterns of the cathode at fully discharged states after 200 cycles under different charging rates. In general, the layered structure of the NMC materials is well maintained when fitted with the  $R\overline{3}m$  [166] space group. However, peak shifting and intensity changes can still be noticed. For example, Figure 2b shows the local magnification of (108) and (110) peaks which are directly related to the a and c value of the unit cell. The shifting of (108) to lower d spacing while (110) shifting to higher d spacing with increasing charging rates indicates the increase of c and decrease of a. This is also shown in Figure 2c of the unit cell parameters derived from the refinement of neutron diffraction data. The structural expansion along c direction indicates the loss of Li ions in the lithium slabs which increases the repulsive force between adjacent oxygen slabs. The increase of c with the increase of charging rates indicates less Li ion inventory available for faster charging after long-term cycles. Bond length information is shown in Figure 2d, and the absolute values of the bond lengths reveal only slight changes from

pristine state to fully discharged states after repeated cycling. However, the trend in changes can be explained by the loss of Li inventory in the Li ion slab, and these changes demonstrate the fast charging at 6C rate leads to the most Li loss after cycling. Figure S1 shows the neutron powder diffraction of graphite after 200 cycles. The diffraction patterns are the same as pristine graphite and can be indexed to space group P6<sub>3</sub>/mmc. This demonstrates electrode structural changes mainly occurs in the cathode materials during cell aging, which is consistent with previous reports [34,35].



**Figure 2**. (a) Neutron power diffraction and the Rietveld refinement fitting to the curves. (b) Diffraction patterns showing the shifting of (108) and (110) peaks. (c) Lattice parameters of a and c from the Rietveld refinement. (d) Ni-O, Li-O, O-O intra layer, and O-O interlayer bond lengths.



**Figure 3.** Voltage curves of Li coin cells assembled with NMC622 cathode after 200 cycles under +1C/-1C, +4C/-1C and +6C/-1C charge/discharge rates. The material was delithiated first and then lithiated at a constant rate of C/10 between 2.5 and 4.2 V.

To confirm the Li inventory loss after long-term cycling and evaluate the reversibility of the cathode structures, coin cells were made from the aged NMC622 cathodes with fresh Li counter electrodes and electrolyte as shown in **Figure 3**. The cells were charged and then discharged to assess the Li inventory left in the structure and Li ions that can be intercalated back. The 1<sup>st</sup> charge capacities of the cells are 161, 156, and 115 mAh/g for 1C, 4C and 6C, respectively. This is in accordance with the neutron diffraction result that higher charging rate leads to more Li inventory loss during cycling. However, all the three cells show similar discharge capacity of 171-175

mAh/g, indicating the reversibility of the cathode structure for Li intercalation/de-intercalation is not affected by fast charging. Figure S2 shows the voltage curves of the aged graphite electrodes in reassembled Li coin cells, which overlaps well with each other regardless of the charging rates during pouch cell aging. This indicates the graphite electrode has good structural integrity without exfoliation or disordering from rapid lithium intercalation during fast charging.

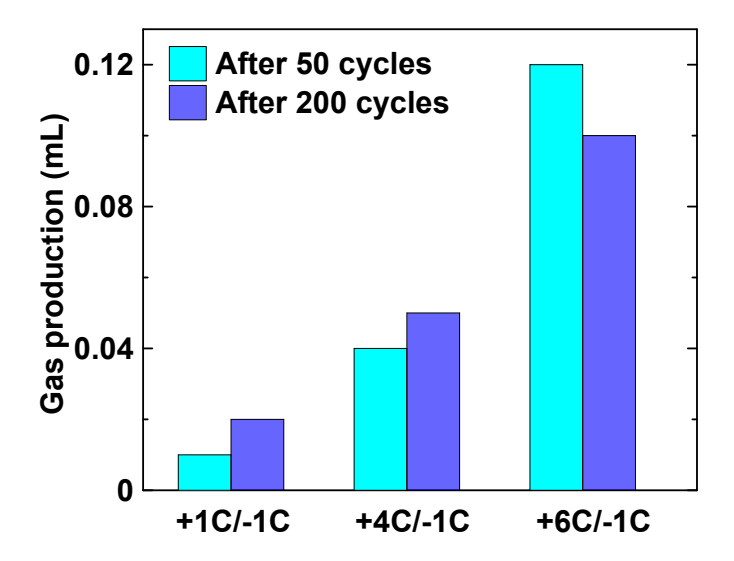


**Figure 4**. Comparison of the gas volume measured by Archimedes' principle under different charging rates. The pouch cells have an initial cell volume of ~4.0 mL.

**Figure 4** shows the gas production of the cells after 50<sup>th</sup> and 200<sup>th</sup> cycles under different charging rates. Gas generation during cell aging is mainly from the decomposition of the electrolyte at the electrode/electrolyte interfaces [36–38]. A general trend in **Figure 4** is that the gas production increases with the increase of charging rate. The cell under +6C/-1C charge/discharge rate shows more gas production after 50 cycles than after 200 cycles. We believe this phenomenon can be explained by the cathode-anode cross-talk during cell aging. The gas generated from one electrode can migrate to the other electrode, and the gas generated in initial cycles can be gradually consumed in the following cycles, either electrochemically or chemically [39–41]. In this study,

the scale of the gas production is relatively small (0.02-0.12 mL) compared to the total cell volume of ~4.0 mL. This is also the case in previous report when cells were cycled at a moderate rate (C/3) [28]. Therefore, gas production in the cells is not considered as an issue for fast charging of the cells within normal voltage range (2.8-4.2 V).

**Figure 5** shows Li ion molarity in electrolytes from ICP-OES measurement after 200 cycles under different charging rates. The molarity is slightly increased in all three cases, which contrasts with the report by Thompson et al. which shows a slight decrease in molarity for cells cycled at a moderate rate of C/3 [28]. This suggests that the solvent has been consumed at a slightly higher rate compared to Li ions in the cells. Nonetheless, the relative change of the Li molarity is small (within 8%). Transition metal ion concentration was also measured in the ICP-OES test, all the three elements (Ni, Co and Mn) were below 10 ppm or detection limits. Therefore, fast charging has no impact on the transition metal ion dissolution from the crystal structure.

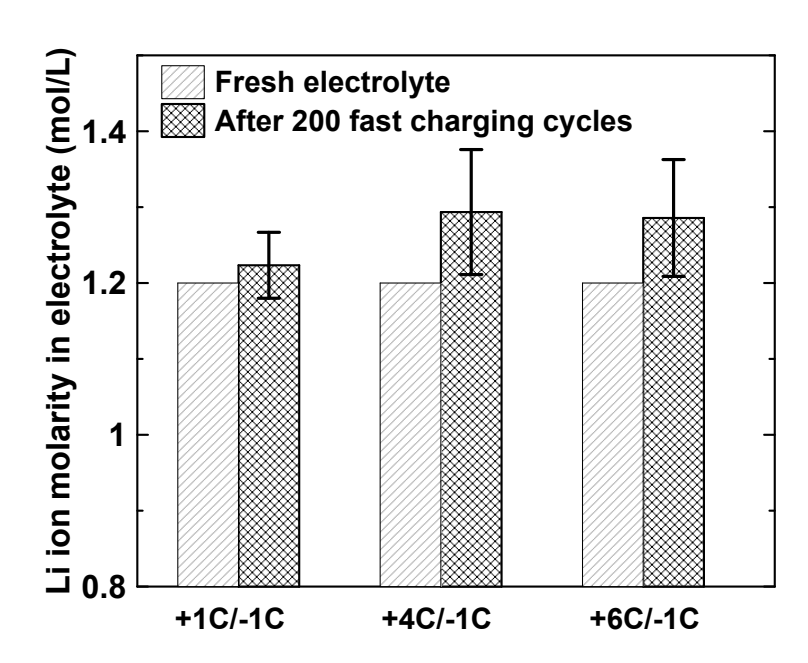


**Figure 5.** Changes in Li ion molarity in the electrolyte after 200 cycles under different charging rates.

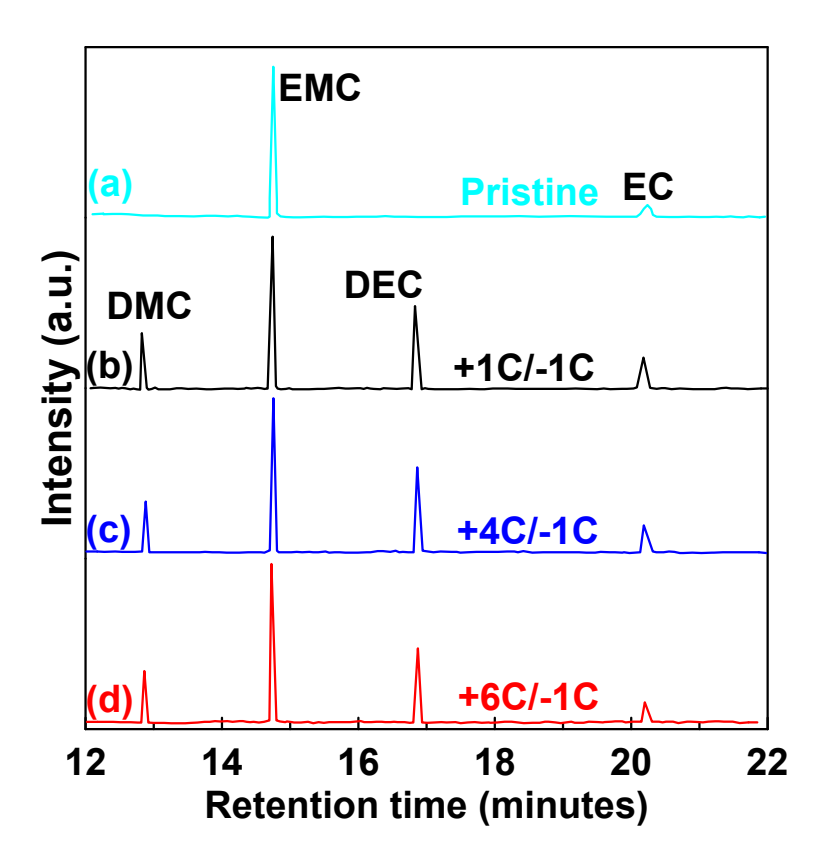


**Figure 6.** Chromatogram of (a) pristine electrolyte, (b) electrolyte after 200 +1C/-1C cycles, (c) electrolyte after 200 +4C/-1C cycles, (d) electrolyte after 200 +6C/-1C cycles.

**Figure 6** shows the corresponding chromatograms of different electrolyte samples analyzed by GC-MS. The carrying solvent, dichloromethane, has a huge peak at a retention time of 10.65 minutes, and was not included in this figure for better clarity on the carbonate solvents in Li-ion electrolyte. In conjunction with MS analysis (Figure S3) on the retention peaks, the following peaks are assigned to dimethyl carbonate (DMC), EMC, diethyl carbonate (DEC) and EC at 12.80, 14.75, 16.80, and 20.20 minutes, respectively. In the pristine electrolyte sample, only EMC and EC are presented in Figure 6a, in consistent with its constituents. However, DMC and DEC are generated via the transesterification of EMC after repeated cycles in all cases under different charging rate. The presence of Li-alkoxides, one of the reduction products from EMC on anode/electrolyte interface, is speculated to facilitate the transesterification reaction as firstly

reported by Yoshida et al. [42]. This transesterification has been extensively reported in cells with slow and/or moderate charging rates [28,29,43]. Although the GC-MS method used in this study is semiquantitative, the tentative conclusion is that transesterification decrease with the increase of charging rate. This agrees with previous report that electrolyte reduction (SEI growth) follows a parabolic growth law [22], which means time, not cycle count, dominates the parasitic reaction. With cycling counts the same, faster charging rate has less time in total, which, in turn, leads to less transesterification in the electrolyte.

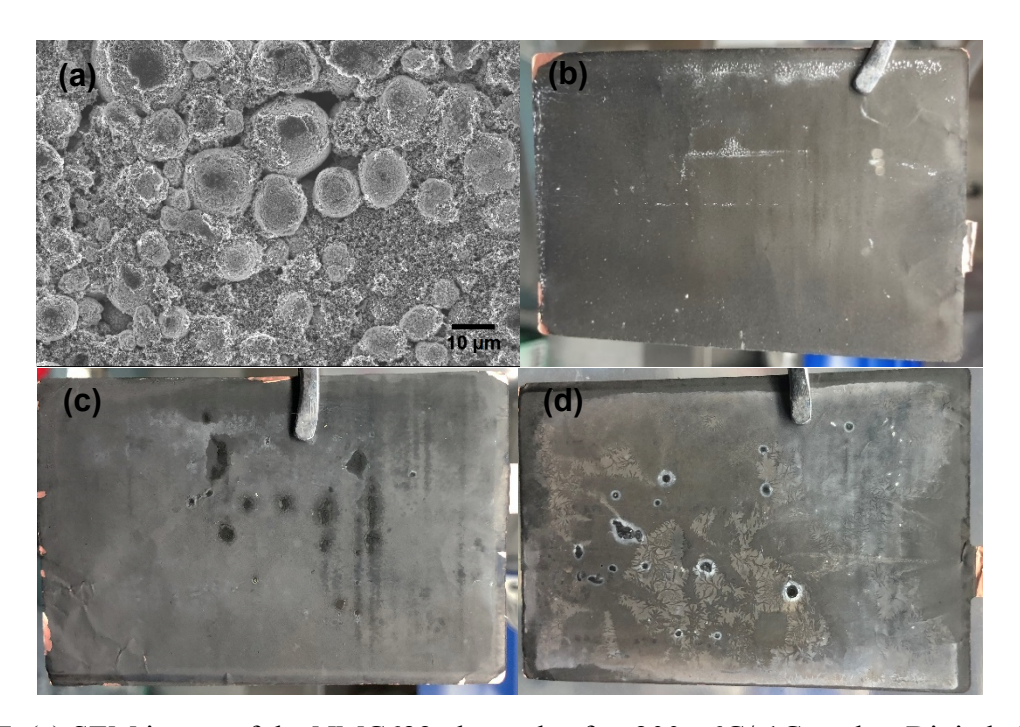


**Figure 7.** (a) SEM image of the NMC622 electrode after 200 +6C/-1C cycles. Digital photos of the graphite electrodes after 200 cycles under (b) +1C/-1C, (c) +4C/-1C, and (d) +6C/-1C, respectively.

**Figure 7a** shows the morphology of the NMC622 cathode after 200 +6C/-1C cycles. NMC622 secondary particles dispersed well in the carbon black matrix with good structural integrity. This SEM image has little difference from the electrodes after 200 cycles under +1C/-1C or +4C/-1C rates (Figure S4). As discussed above, the capacity loss is mainly from the Li inventory loss in the

layered crystal structures, not from loss of active material. **Figure 7**b, c and d show the digital photos of the graphite electrodes after 200 cycles under +1C/-1C, +4C/-1C and +6C/-1C, respectively. The cells were disassembled at fully discharged state and was kept inside the Arfilled glove box. The surface color changed from the grey of graphite for +1C/-1C to pale white for +6C/-1C, with the +4C/-1C in-between. This is in consistent with the cycling performance in **Figure 1**. With the increase of charging rate, more capacity fading is observed due to Li ion mass transport limitation [11,30,44]. Metallic Li plating leads to more parasitic reaction due to its high reactivity and "dead" lithium from electrical disconnection to graphite electrode. This also explains the Li inventory loss in the cathode in **Figure 2**, which converted into the Li plating in high charging rate cells.

## Conclusion

Pouch cells with a moderate loading of 2.3 mAh/cm² were tested under different charging rates at 1C, 4C and 6C to evaluate its fast charging capabilities. Rapid capacity deterioration was observed for extreme fast charging (6C) cells with only 73.8% capacity retention after 200 cycles compared to 94.0% and 89.4% for 1C and 4C, respectively. An increasing portion of capacity for 6C was obtained from the high voltage (4.2V) trickle charging. Post-mortem analysis on the cathode materials indicated Li inventory loss from the Li slab in the layered structure with a shrinkage of *a* and expansion of *c*. Li coin cell test using the aged NMC622 electrodes confirmed the Li loss. However, the cathode structure was not compromised as Li can be reversibly intercalated/deintercalated in the structure once the Li inventory was replenished. The electrolyte in the aged cells showed a slight increase of Li molarity, indicating a higher consuming rate of solvent compared to Li salt in the electrolyte. GC-MS analysis on the electrolyte solvents observed less transesterification when higher charging rate was applied, which was attributed to the less charge

time for higher charging rate. Metallic Li plating was severer at higher charging rate, which accounted for the Li inventory loss in the cell. These findings deepen the understanding on cell aging mechanism when fast charging was applied and can be used as benchmarks for future improvement studies.

## Acknowledgement

This research at Oak Ridge National Laboratory, managed by UT Battelle, LLC, for the U.S. Department of Energy (DOE) under contract DE-AC05-00OR22725, was sponsored by the Office of Energy Efficiency and Renewable Energy (EERE) Vehicle Technologies Office (VTO) (Technology Manager: Brian Cunningham). Neutron diffraction in this research used resources at the Spallation Neutron Source, a DOE Office of Science User Facility operated by the Oak Ridge National Laboratory. SEM was conducted at the Center for Nanophase Materials Sciences, which is a DOE Office of Science User Facility.

#### **References:**

- [1] Z.A. Needell, J. McNerney, M.T. Chang, J.E. Trancik, Potential for widespread electrification of personal vehicle travel in the United States, Nat. Energy. 1 (2016) 16112. https://doi.org/10.1038/nenergy.2016.112.
- [2] S. Ahmed, I. Bloom, A.N. Jansen, T. Tanim, E.J. Dufek, A. Pesaran, A. Burnham, R.B. Carlson, F. Dias, K. Hardy, M. Keyser, C. Kreuzer, A. Markel, A. Meintz, C. Michelbacher, M. Mohanpurkar, P.A. Nelson, D.C. Robertson, D. Scoffield, M. Shirk, T. Stephens, R. Vijayagopal, J. Zhang, Enabling fast charging A battery technology gap assessment, J. Power Sources. 367 (2017) 250–262. https://doi.org/10.1016/j.jpowsour.2017.06.055.

- [3] Q. Liu, C. Du, B. Shen, P. Zuo, X. Cheng, Y. Ma, G. Yin, Y. Gao, Understanding undesirable anode lithium plating issues in lithium-ion batteries, RSC Adv. 6 (2016) 88683–88700. https://doi.org/10.1039/c6ra19482f.
- [4] T. Waldmann, B.I. Hogg, M. Wohlfahrt-Mehrens, Li plating as unwanted side reaction in commercial Li-ion cells A review, J. Power Sources. 384 (2018) 107–124. https://doi.org/10.1016/j.jpowsour.2018.02.063.
- [5] C. Pastor-Fernández, K. Uddin, G.H. Chouchelamane, W.D. Widanage, J. Marco, A Comparison between Electrochemical Impedance Spectroscopy and Incremental Capacity-Differential Voltage as Li-ion Diagnostic Techniques to Identify and Quantify the Effects of Degradation Modes within Battery Management Systems, J. Power Sources. 360 (2017) 301–318. https://doi.org/10.1016/j.jpowsour.2017.03.042.
- [6] J. Liu, Q. Duan, M. Ma, C. Zhao, J. Sun, Q. Wang, Aging mechanisms and thermal stability of aged commercial 18650 lithium ion battery induced by slight overcharging cycling, J. Power Sources. 445 (2020) 227263. https://doi.org/10.1016/j.jpowsour.2019.227263.
- [7] Y. Gao, J. Jiang, C. Zhang, W. Zhang, Z. Ma, Y. Jiang, Lithium-ion battery aging mechanisms and life model under different charging stresses, J. Power Sources. 356 (2017) 103–114. https://doi.org/10.1016/j.jpowsour.2017.04.084.
- [8] J.C. Burns, D.A. Stevens, J.R. Dahn, In-Situ Detection of Lithium Plating Using High Precision Coulometry, J. Electrochem. Soc. 162 (2015) A959–A964. https://doi.org/10.1149/2.0621506jes.
- [9] C. Uhlmann, J. Illig, M. Ender, R. Schuster, E. Ivers-Tiffée, In situ detection of lithium

- metal plating on graphite in experimental cells, J. Power Sources. 279 (2015) 428–438. https://doi.org/10.1016/j.jpowsour.2015.01.046.
- [10] S.S. Zhang, K. Xu, T.R. Jow, Study of the charging process of a LiCoO2-based Li-ion battery, J. Power Sources. 160 (2006) 1349–1354.
  https://doi.org/10.1016/j.jpowsour.2006.02.087.
- [11] K.G. Gallagher, S.E. Trask, C. Bauer, T. Woehrle, S.F. Lux, M. Tschech, P. Lamp, B.J. Polzin, S. Ha, B. Long, Q. Wu, W. Lu, D.W. Dees, A.N. Jansen, Optimizing Areal Capacities through Understanding the Limitations of Lithium-Ion Electrodes, J. Electrochem. Soc. 163 (2016) A138–A149. https://doi.org/10.1149/2.0321602jes.
- [12] A.J. Smith, J.C. Burns, D. Xiong, J.R. Dahn, Interpreting High Precision Coulometry Results on Li-ion Cells, J. Electrochem. Soc. 158 (2011) A1136. https://doi.org/10.1149/1.3625232.
- [13] F. Ding, W. Xu, X. Chen, J. Zhang, M.H. Engelhard, Y. Zhang, B.R. Johnson, J. V. Crum, T.A. Blake, X. Liu, J.-G. Zhang, Effects of Carbonate Solvents and Lithium Salts on Morphology and Coulombic Efficiency of Lithium Electrode, J. Electrochem. Soc. 160 (2013) A1894–A1901. https://doi.org/10.1149/2.100310jes.
- [14] D. Aurbach, E. Zinigrad, H. Teller, P. Dan, Factors Which Limit the Cycle Life of Rechargeable Lithium (Metal) Batteries, J. Electrochem. Soc. 147 (2000) 1274. https://doi.org/10.1149/1.1393349.
- [15] R. Weber, M. Genovese, A.J. Louli, S. Hames, C. Martin, I.G. Hill, J.R. Dahn, Long cycle life and dendrite-free lithium morphology in anode-free lithium pouch cells enabled by a dual-salt liquid electrolyte, Nat. Energy. 4 (2019) 683–689.

- https://doi.org/10.1038/s41560-019-0428-9.
- [16] M. Broussely, P. Biensan, F. Bonhomme, P. Blanchard, S. Herreyre, K. Nechev, R.J. Staniewicz, Main aging mechanisms in Li ion batteries, J. Power Sources. 146 (2005) 90–96. https://doi.org/10.1016/j.jpowsour.2005.03.172.
- [17] Z. Li, J. Huang, B. Yann Liaw, V. Metzler, J. Zhang, A review of lithium deposition in lithium-ion and lithium metal secondary batteries, J. Power Sources. 254 (2014) 168–182. https://doi.org/10.1016/j.jpowsour.2013.12.099.
- [18] X. Zhu, Z. Wang, C. Wang, L. Huang, Overcharge Investigation of Large Format Lithium-Ion Pouch Cells with Li(Ni 0.6 Co 0.2 Mn 0.2) O 2 Cathode for Electric Vehicles: Degradation and Failure Mechanisms, J. Electrochem. Soc. 165 (2018) A3613– A3629. https://doi.org/10.1149/2.0161816jes.
- [19] X. Zhu, H. Wang, S. Allu, Y. Gao, E. Cakmak, E.J. Hopkins, G.M. Veith, Z. Wang, Investigation on capacity loss mechanisms of lithium-ion pouch cells under mechanical indentation conditions, J. Power Sources. 465 (2020) 228314. https://doi.org/10.1016/j.jpowsour.2020.228314.
- [20] S. Huang, X. Wu, G.M. Cavalheiro, X. Du, B. Liu, Z. Du, G. Zhang, In Situ Measurement of Lithium-Ion Cell Internal Temperatures during Extreme Fast Charging, J. Electrochem. Soc. 166 (2019) 3254–3259. https://doi.org/10.1149/2.0441914jes.
- [21] X.-G. Yang, G. Zhang, S. Ge, C.-Y. Wang, Fast charging of lithium-ion batteries at all temperatures, Proc. Natl. Acad. Sci. 115 (2018) 7266–7271. https://doi.org/10.1073/pnas.1807115115.

- [22] A.J. Smith, J.C. Burns, X. Zhao, D. Xiong, J.R. Dahn, A High Precision Coulometry Study of the SEI Growth in Li/Graphite Cells, J. Electrochem. Soc. 158 (2011) A447. https://doi.org/10.1149/1.3557892.
- [23] J. Vetter, P. Novák, M.R. Wagner, C. Veit, K.-C. Möller, J.O. Besenhard, M. Winter, M. Wohlfahrt-Mehrens, C. Vogler, A. Hammouche, Ageing mechanisms in lithium-ion batteries, J. Power Sources. 147 (2005) 269–281.
  https://doi.org/10.1016/j.jpowsour.2005.01.006.
- [24] T. Waldmann, M. Wilka, M. Kasper, M. Fleischhammer, M. Wohlfahrt-Mehrens, Temperature dependent ageing mechanisms in Lithium-ion batteries – A Post-Mortem study, J. Power Sources. 262 (2014) 129–135. https://doi.org/10.1016/j.jpowsour.2014.03.112.
- [25] J. Neuefeind, M. Feygenson, J. Carruth, R. Hoffmann, K.K. Chipley, The Nanoscale Ordered MAterials Diffractometer NOMAD at the Spallation Neutron Source SNS, Nucl. Instruments Methods Phys. Res. Sect. B Beam Interact. with Mater. Atoms. 287 (2012) 68–75. https://doi.org/10.1016/j.nimb.2012.05.037.
- [26] A.A. Coelho, P.A. Chater, A. Kern, Fast synthesis and refinement of the atomic pair distribution function, J. Appl. Crystallogr. 48 (2015) 869–875. https://doi.org/10.1107/S1600576715007487.
- [27] J. Self, C.P. Aiken, R. Petibon, J.R. Dahn, Survey of Gas Expansion in Li-Ion NMC Pouch Cells, J. Electrochem. Soc. 162 (2015) A796–A802. https://doi.org/10.1149/2.0081506jes.
- [28] L.M. Thompson, W. Stone, A. Eldesoky, N.K. Smith, C.R.M. McFarlane, J.S. Kim, M.B.

- Johnson, R. Petibon, J.R. Dahn, Quantifying Changes to the Electrolyte and Negative Electrode in Aged NMC532/Graphite Lithium-Ion Cells, J. Electrochem. Soc. 165 (2018) A2732–A2740. https://doi.org/10.1149/2.0721811jes.
- [29] R. Petibon, L. Rotermund, K.J. Nelson, A.S. Gozdz, J. Xia, J.R. Dahn, Study of Electrolyte Components in Li Ion Cells Using Liquid-Liquid Extraction and Gas Chromatography Coupled with Mass Spectrometry, J. Electrochem. Soc. 161 (2014) A1167–A1172. https://doi.org/10.1149/2.117406jes.
- [30] Z. Du, D.L. Wood, C. Daniel, S. Kalnaus, J. Li, Understanding limiting factors in thick electrode performance as applied to high energy density Li-ion batteries, J. Appl. Electrochem. 47 (2017) 405–415. https://doi.org/10.1007/s10800-017-1047-4.
- [31] Q.Q. Liu, R. Petibon, C.Y. Du, J.R. Dahn, Effects of Electrolyte Additives and Solvents on Unwanted Lithium Plating in Lithium-Ion Cells, J. Electrochem. Soc. 164 (2017) A1173–A1183. https://doi.org/10.1149/2.1081706jes.
- [32] S.S. Choi, H.S. Lim, Factors that affect cycle-life and possible degradation mechanisms of a Li-ion cell based on LiCoO2, J. Power Sources. 111 (2002) 130–136. https://doi.org/10.1016/S0378-7753(02)00305-1.
- [33] J.C. Burns, N.N. Sinha, D.J. Coyle, G. Jain, C.M. VanElzen, W.M. Lamanna, A. Xiao, E. Scott, J.P. Gardner, J.R. Dahn, The Impact of Varying the Concentration of Vinylene Carbonate Electrolyte Additive in Wound Li-Ion Cells, J. Electrochem. Soc. 159 (2011) A85–A90. https://doi.org/10.1149/2.028202jes.
- [34] S.S. Zhang, Unveiling Capacity Degradation Mechanism of Li-ion Battery in Fast-charging Process, ChemElectroChem. 7 (2020) 555–560.

- https://doi.org/10.1002/celc.201902050.
- [35] A.S. Mussa, A. Liivat, F. Marzano, M. Klett, B. Philippe, C. Tengstedt, G. Lindbergh, K. Edström, R.W. Lindström, P. Svens, Fast-charging effects on ageing for energy-optimized automotive LiNi1/3Mn1/3Co1/3O2/graphite prismatic lithium-ion cells, J. Power Sources. 422 (2019) 175–184. https://doi.org/10.1016/j.jpowsour.2019.02.095.
- [36] K. Kumai, H. Miyashiro, Y. Kobayashi, K. Takei, R. Ishikawa, Gas generation mechanism due to electrolyte decomposition in commercial lithium-ion cell, J. Power Sources. (1999). https://doi.org/10.1016/S0378-7753(98)00234-1.
- [37] X. Teng, C. Zhan, Y. Bai, L. Ma, Q. Liu, C. Wu, F. Wu, Y. Yang, J. Lu, K. Amine, In Situ Analysis of Gas Generation in Lithium-Ion Batteries with Different Carbonate-Based Electrolytes, ACS Appl. Mater. Interfaces. (2015). https://doi.org/10.1021/acsami.5b08399.
- [38] N.E. Galushkin, N.N. Yazvinskaya, D.N. Galushkin, Mechanism of Gases Generation during Lithium-Ion Batteries Cycling, J. Electrochem. Soc. 166 (2019) A897–A908. https://doi.org/10.1149/2.0041906jes.
- [39] D.J. Xiong, L.D. Ellis, R. Petibon, T. Hynes, Q.Q. Liu, J.R. Dahn, Studies of Gas Generation, Gas Consumption and Impedance Growth in Li-Ion Cells with Carbonate or Fluorinated Electrolytes Using the Pouch Bag Method, J. Electrochem. Soc. 164 (2017) A340–A347. https://doi.org/10.1149/2.1091702jes.
- [40] L.D. Ellis, J.P. Allen, L.M. Thompson, J.E. Harlow, W.J. Stone, I.G. Hill, J.R. Dahn, Quantifying, Understanding and Evaluating the Effects of Gas Consumption in Lithium-Ion Cells, J. Electrochem. Soc. 164 (2017) A3518–A3528.

- https://doi.org/10.1149/2.0191714jes.
- [41] C. Mao, R.E. Ruther, L. Geng, Z. Li, D.N. Leonard, H.M. Meyer, R.L. Sacci, D.L. Wood, Evaluation of Gas Formation and Consumption Driven by Crossover Effect in High-Voltage Lithium-Ion Batteries with Ni-Rich NMC Cathodes, ACS Appl. Mater.

  Interfaces. 11 (2019) 43235–43243. https://doi.org/10.1021/acsami.9b15916.
- [42] H. Yoshida, T. Fukunaga, T. Hazama, M. Terasaki, M. Mizutani, M. Yamachi,
  Degradation mechanism of alkyl carbonate solvents used in lithium-ion cells during initial
  charging, J. Power Sources. 68 (1997) 311–315. https://doi.org/10.1016/S03787753(97)02635-9.
- [43] H. Kim, S. Grugeon, G. Gachot, M. Armand, L. Sannier, S. Laruelle, Ethylene biscarbonates as telltales of SEI and electrolyte health, role of carbonate type and new additives, Electrochim. Acta. 136 (2014) 157–165. https://doi.org/10.1016/j.electacta.2014.05.072.
- [44] Z. Du, D.L. Wood, I. Belharouak, Enabling fast charging of high energy density Li-ion cells with high lithium ion transport electrolytes, Electrochem. Commun. 103 (2019) 109–113. https://doi.org/10.1016/j.elecom.2019.04.013.